Enhancing Methanol Oxidation Reaction with Platinum-Ruthenium Embedded MXene: Synthesis, Characterization, and Electrochemical Properties

Norulsamani Abdullah[1,2*], R. Saidur[1,2,3], Azran Mohd Zainoodin[4], Kim Han Tan[1], Adarsh Kumar Pandey[1]

[1]*Research Center for Nano-Materials and Energy Technology (RCNMET), School of Engineering and Technology, Sunway University, Bandar Sunway, Petaling Jaya, 47500, Selangor Darul Ehsan, Malaysia*
[2]*Sunway Materials Smart Science & Engineering (SMS2E) Cluster, Sunway University, Petaling Jaya, Selangor, 47500, Malaysia*
[3]*School of Engineering, Lancaster University, Lancaster, LA1 4YW, UK*
[4]*Fuel Cell Institute, UniversitiKebangsaan Malaysia, 43600 UKM Bangi, Selangor, Malaysia*

Corresponding authors: nabdullah@sunway.edu.my

ABSTRACT

Methanol oxidation reaction (MOR) is the main reaction that takes place in an anodic electrode of a direct methanol fuel cell (DMFC), whichis a promising electrochemical energy conversion technology. This study presents a novel approach for enhancing the electrocatalytic activity of MOR performance using composite of MXene ($Ti_3C_2T_x$) with Pt and Ru bimetal. The aim of this study is to investigate the optimum electrocatalyst loading for PtRu/$Ti_3C_2T_x$ to improve and stand out the potential of electrocatalysts in the MOR catalytic activity. The study also provides detailed physical characterizations and electrochemical measurements. The results show that the electrocatalyst loading of 0.40 $mgcm^{-2}$ has the highest ECSA value and better reaction activity compared to other loadings. The electrocatalytic activity, CO tolerance, and stability of the electrocatalyst also show the better result for this loading. The comparative study with previous research shows that the PtRu/$Ti_3C_2T_x$ electrocatalyst exhibits the highest catalytic activity, which is 5.13 times better than that of the previous study on the Pt/C electrocatalyst. Thus, the novel combination of MXene structure and PtRu indicates a promising electrocatalyst for MOR.

Keywords: MXene; Electrocatalyst; Electrochemical properties; Methanol oxidation reaction; Affordable and clean energy.

GRAPHICAL ABSTRACT

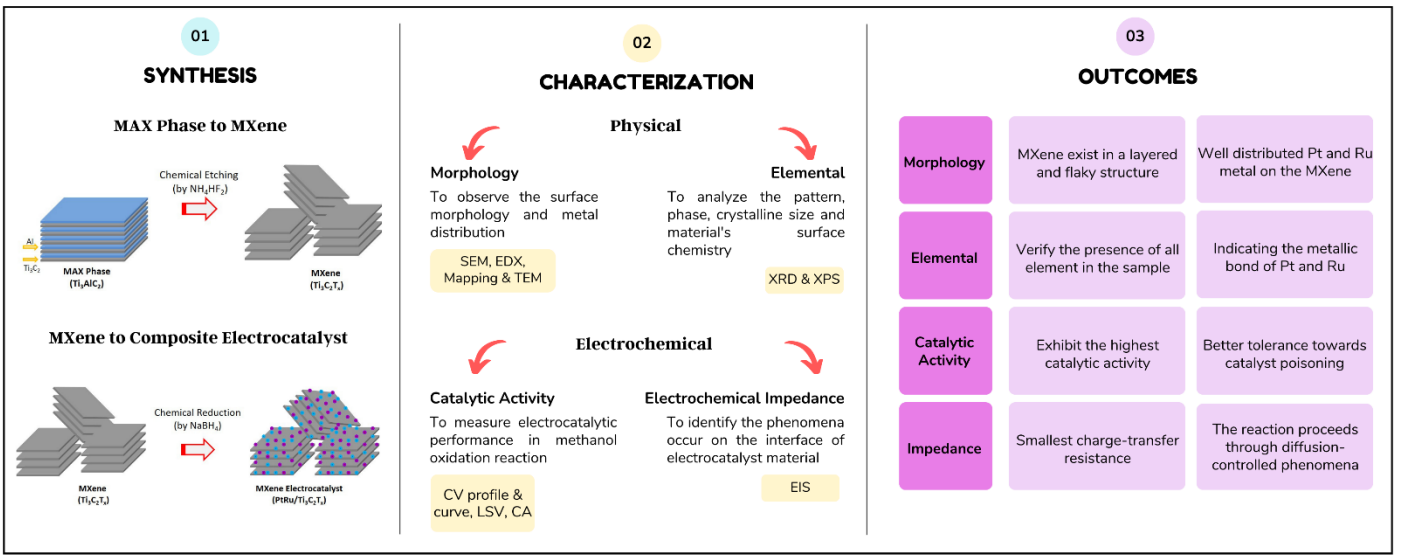

1. INTRODUCTION

Since the industrial revolution in the 18th century, various technological inventions and developments have been achieved to increase the use of technology in daily life and to provide survival in this challenging world. However, the breakthrough in technology has resulted in surplus products leading to environmental pollution, climate change, natural resource depletion and many other environmental issues. This not only affects a particular country but also covers the whole world which will be the lifeblood of future generations. Therefore, the United Nations (UN) general assembly declared the decade between 2014 – 2024 as the '*Decade of sustainable energy for all*' and encourage sustainable development in developing nations [1]. The UN has formulated 17 sustainable development goals (SDGs) to encourage sustainable development worldwide, and

researchers globally are actively working towards these goals. Malaysia is also committed to contributing to the creation of a sustainable environment, as evidenced by its 'National Green Technology Policy'. This policy advocates for the promotion and adoption of green technology and renewable energy approaches as the key solutions towards achieving sustainable development [2]. Therefore, this study is contributed towards the SDG 7; ‘Affordable and Clean Energy’.

Among all the approaches, fuel cell technology is one of the most outstanding that comes out with various types for various applications including direct methanol fuel cell (DMFC) that focused on portable devices like mobile phones, notebook computers and other devices [3]. This technology can also be used as a replacement for batteries [4]. DMFC offers many advantages, such as having a simple system design, generating high specific energy, the high-energy density of methanol, low operating temperature, easy start-up and being classified as a zero-emission of power source system [5]. However, this technology needs to overcome several challenges that hindering from commercialization. Among them are methanol crossover, low power density, and slow kinetics of methanol oxidation reaction (MOR) [4]. Apart from methanol crossover, the catalyst issue is a major challenge. The catalyst is the ‘heart’ of the fuel cell that is present in the membrane electrode assembly (MEA) at the anodic and cathodic parts. The slow kinetics of MOR is due to the low activity of methanol oxidation and high CO poisoning level which involves the anodic electrocatalyst [6]. This problem gives a high impact on the overall DMFC performance. Thus, this study is focused on the kinetics problem of MOR in DMFC via developing and modifying the electrocatalyst for the anodic part.

There are several avenues have been explored to overcome the challenges, which are decreasing electrocatalyst particle size, developing binary and ternary electrocatalyst composite, improving electrocatalyst dispersion, as well as enhanced catalyst support materials. Yang et al.

[7] studied the polymer-coated carbon black as an anodic electrocatalyst and found that the electrocatalyst hasthe highest mass activity of the MOR among the recorded catalytic activities of carbon black-based electrocatalyst. Anitha et al. [8] investigated the TiO_2 nanotube layers (TNTs) decorated with Pt nanoparticles for anodic electrocatalytic activity. The result revealed that the TNTs catalyst support was homogeneously distributed on Pt nanoparticles and produceda high surface area, which leads to high-performance electrocatalysis. Xei et al. [9] prepared Pt/C@NiRuCe layered double hydroxide electrocatalyst for the methanol electrooxidation. The result showed that the charge transfer and catalytic activity of the electrocatalyst were influenced by the additional cerium-doped, which possesses the best electrocatalytic performance.

The addition or modification of material as one of the elements in the composite anodic electrocatalyst becomes the main interest among DMFC researchers [10-13]. PtRu is widely recognized for having the highest catalytic activity for MOR, and its benefits are widely acknowledged [14-17]. Pt, in particular, has been shown to exhibit exceptional catalytic activity, chemical stability, and superior work function [18]. Meanwhile, Ru can give the electron effect or a bi-functional mechanism that causesthe CO to become weakly adsorbed and reduces the catalyst poisoning [19]. However, the DMFC still faces slow kinetics, low efficiency, and high cost that leads to the catalyst issue [19]. Therefore, MXene with a unique two-dimensional (2D) structure are capable of providing a fast ion/charge transfer path [20], excellent electric conductivity and strong binding strength [21, 22] are expected to function as the ternary catalyst element with Pt and Ru in DMFC. The outstanding properties of MXene are predicted to be beneficial in increasing the active catalytic sites for MOR [20, 23], weakening the CO adsorption, and increasing the reaction activity. This will assist the low activity and electrocatalyst poisoning problems in the MOR.

This paper reported the formulation of PtRu with $Ti_3C_2T_x$ as an anodic electrocatalyst for application in DMFC technology. This is the first work to report the optimum PtRu/$Ti_3C_2T_x$ electrocatalyst loading for the MOR. The physical characterization of electrocatalyst involving morphology and material distribution is analyzed using field emission scanning electron microscopy (FESEM), energy dispersive x-ray (EDX), scanning electron microscopy (SEM), mapping and transmission electron microscopy (TEM) analysis. The detail of elemental and material surface chemistry using x-ray diffraction (XRD) and x-ray photoelectron spectroscopy (XPS) analysis for both materials of $Ti_3C_2T_x$ and PtRu/$Ti_3C_2T_x$ is also the first time reported to be discussed. The electrochemical active surface area (ECSA), Tafel analysis,electrocatalytic activity, CO tolerance, and electrochemical impedance for MOR are measured in this study. The chronoamperometry (CA) as stability measurement is evaluated for PtRu/$Ti_3C_2T_x$ in MOR which was also reported for the first time. The 0.40 $mgcm^{-2}$ electrocatalyst loading is found to have the highest ECSA value of 54.91 $m^2g_{Pt}^{-1}$. The Tafel analysis for this loading also shows to be the highest and better reaction activity compared to other electrocatalyst loadings. In addition, the electrocatalytic activity and CO tolerance for this loading also show the highest value compared to other samples. Other than that, this loading shows the smallest semicircle arc in electrochemical impedance measurement that indicates the lowest charge-transfer resistance with good stability for long performance measurement. The study was compared with a previous study of the electrocatalytic performance of DMFC commercial electrocatalyst, Pt/C, and found that PtRu/$Ti_3C_2T_x$ is 5.13 times higher in the current density value. This is another excellent finding for this study that indicates the potential of the PtRu/$Ti_3C_2T_x$ electrocatalyst for MOR activity.

2. EXPERIMENTAL

2.1 Materials and Chemicals

The following materials were used to synthesize $Ti_3C_2T_x$, and PtRu/$Ti_3C_2T_x$ electrocatalyst as well as preparation of electrochemical measurement. Ti_3AlC_2 MAX phase material (Y-Carbon Ltd.), ammonium hydrogen difluoride (NH_4HF_2) etching agent (reagent grade 95 %, Sigma Aldrich), sodium hydroxide (NaOH, 97 % purity, Sigma Aldrich) and dimethyl sulfoxide (DMSO, analytical reagent grade, Fisher Chemicals).The precursor of Pt (H_2PtCl_6, 37.5 % content) and Ru, ($RuCl_3$, 45–55 % content), as well as sodium borohydride ($NaBH_4$, 99 %), were purchased from Sigma Aldrich, Germany. The isopropyl alcohol (IPA, 99.8 %) was obtained from Chemiz, Malaysia. The Nafion solution D520 (5 wt%) was received from Chemours.com and all chemical reagents were used without further purification.

2.2 Preparation of PtRu/$Ti_3C_2T_x$Electrocatalyst

$Ti_3C_2T_x$ was synthesized using NH_4HF_2 as an etching agent and the method was followed by a previous study by Aslfattahi et al. [24]. The etching process is begun with 1 g of Ti_3AlC_2 MAX phase being added slowly into 20 mL of 2 $molL^{-1}$ NH_4HF_2 and stirred for 48 hr at room temperature. After completing the etching process, a dilute NaOH solution was added dropwise until reached pH 6. Then, the solution is centrifuged and washed several times with deionized water. The deposited material is then treated with DMSO for 15 hr at room temperature. The treated solution was centrifuged and washed repeatedly using deionized water, and dried overnight at 70 ^oC. The obtained material can be referred to as $Ti_3C_2T_x$ and will be further used in this study.

The $Ti_3C_2T_x$ acted as a catalyst support, while Pt and Ru as the main catalyst, which produces the electrocatalyst with annotation of PtRu/$Ti_3C_2T_x$. The main catalysts were deposited onto the catalyst support via chemical reduction method, where $NaBH_4$ is used as a reducing agent.

50 mL of IPA, 50 mL of deionized water and 78.9 wt% of $Ti_3C_2T_x$were mixed in a beaker and sonicated for 30 min or until dissolved at room temperature. The composition between $Ti_3C_2T_x$ and PtRu (with a 1:1 atomic ratio) is decided based on our previous study by Abdullah et al. [25]. Then, the Pt and Ru precursors were added and stirred for another 30 min. The pH value was measured and modified using NaOH and HCl until achieved pH 8. The solution temperature was increased up to 80 ^oC, and 25 mL of 0.2 $molL^{-1}$ reducing agent was added drop by drop andstirred continuously for another 1 hr. The solution was cooled, centrifuged and cleansed repeatedly using deionized water. The deposited materials were dried under vacuum conditions for 3 hr at 120 ^oC. The dry material was collected and refined in the mortar and pestle to get the fine powder of $PtRu/Ti_3C_2T_x$ electrocatalyst. The schematic illustration for the material preparation of $PtRu/Ti_3C_2T_x$ is shown in Figure 1.

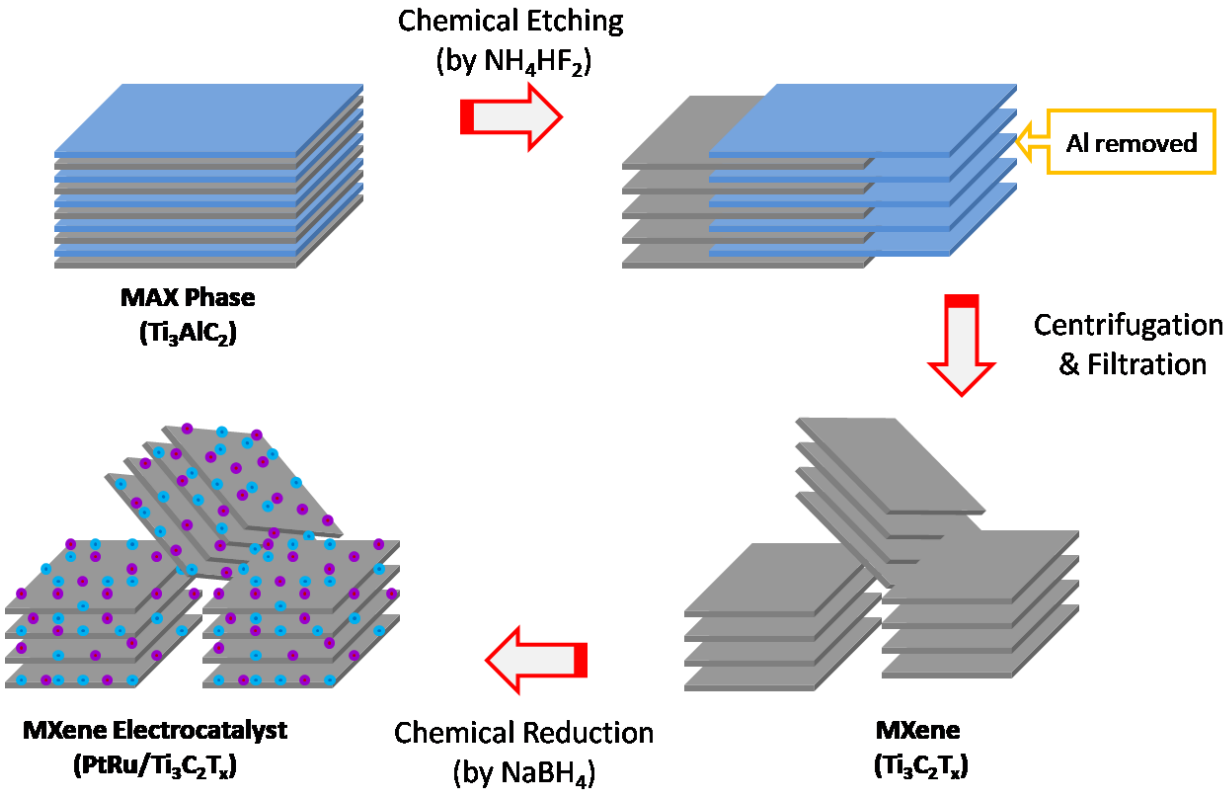

Figure 1: Schematic illustration for the preparation of $PtRu/Ti_3C_2T_x$ electrocatalyst.

2.3 Physical Characterization of PtRu/$Ti_3C_2T_x$ Electrocatalyst

The $Ti_3C_2T_x$and PtRu/$Ti_3C_2T_x$ electrocatalysts were characterized using several analyses to identify physical properties. The FESEM analysis (Hitachi SU8010, Japan) was used to study the surface morphology of both samples, while SEM (TESCAN VEGA3, Czech Republic), EDX and mapping analysis (AZtec analysis software, Oxford Instrument, UK) were used to observe the elemental and distribution of the catalyst decorated on $Ti_3C_2T_x$ catalyst support. Material morphology with high resolution was identified using TEM (Tecnai G^2 20 S-Twin, FEI Company USA).The XRD analysis was performed to analyze the pattern, phase and crystallitesize of the catalyst support and electrocatalyst sample using an x-ray diffractometer (D8 Advance/ Bruker AXS Germany). Further, PtRu/$Ti_3C_2T_x$ electrocatalyst underwent the XPS analysis to analyze the material's surface chemistry using an x-ray photoelectron spectrometer (Kratos – Axis Ultra DLD).

2.4 Electrochemical Measurement

The PtRu/$Ti_3C_2T_x$ electrocatalyst underwent electrochemical measurement to identify the electrochemical properties of the electrocatalyst. The measurements involved were cyclic voltammetry (CV) profile, linear sweep voltammetry (LSV), CV curve, electrochemical impedance spectroscopy (EIS) and chronoamperometry (CA). The CV profile was performed to analyze the ECSA, while LSV was analyzed with the Tafel analysis, charge transfer coefficient and ion exchange current density. Besides, the electrocatalytic performance of MOR and electrocatalyst poisoning effect were measured by the CV curve. The identification of the associated phenomena that occur on the interface of electrocatalyst material is assessed using EIS, while the long-term performance is analyzed by CA measurement. All the electrochemical

measurements were conducted using potentiostat/galvanostat (Interface 1010E; max. applied current (±1 A) and potential (±12 V), Gamry Instruments, USA) with a three-electrode measurement system. The three-electrode consists of glassy carbon (GCE), silver/silver chloride (Ag/AgCl) and Pt electrode that acted as working, reference, and counter electrodes. The working electrode was cleaned using polished paper and alumina suspension before further use in the measurement. Meanwhile, the PtRu/$Ti_3C_2T_x$ electrocatalyst ink was prepared by adding Nafion solution, IPA and deionized water with a ratio of 1: 4.75: 4.75 into the 5 mg of electrocatalyst powder. Then, the mixture was dispersed using a probe sonicator for 15 min or until homogenous at room temperature. The electrocatalyst ink was pipetted onto the 3mm inner diameter of the working electrode surface area. In this study, the electrocatalyst loading of each sample was determined by differentiating the loading of the electrocatalyst ink. The working electrode was dried for 1 hr at room condition before further dried at 80 ^oC for 30 min. Then the electrode was ready to be used in electrochemical measurement with 0.5 $molL^{-1}$ H_2SO_4 in 2.8 $molL^{-1}$ CH_3OH as an electrolyte under a nitrogen environment.

3. RESULTS AND DISCUSSION

3.1 Physical Characterization of PtRu/$Ti_3C_2T_x$ Electrocatalyst

Morphology, elemental and mapping of samples, $Ti_3C_2T_x$ catalyst support and PtRu/$Ti_3C_2T_x$ electrocatalyst were analyzed using FESEM, SEM, EDX and mapping analysis, respectively. Figure 2 (a) and (b) show the FESEM image for catalyst support and electrocatalyst samples at a magnification of 50 kX. This same scale of magnification is provided to gain the clear morphology for both samples. Figure 2 (a) portrays the existence of a layered and some inter-spacing between the layer, which resulted from the broken bond during the selective exfoliation process. The

$Ti_3C_2T_x$ catalyst support also show the flaky structure of multilayer that recognized as a real structure of 2D MXene material. This result is presented by several researchers [24, 26], and it confirms that $Ti_3C_2T_x$ catalyst support was successfully synthesized. The morphology and mapping of the PtRu/$Ti_3C_2T_x$ electrocatalyst are shown in Figure 2 (b). The FESEM image shows the presence of $Ti_3C_2T_x$ catalyst support structure that is fully covered with a small particle. The small particle is expected to be a metal of Pt and Ru, which is a result from the chemical reduction method during the synthesis of PtRu/$Ti_3C_2T_x$. The metal is seen to be distributed well on the surface of the $Ti_3C_2T_x$ catalyst support.

However, to get the confirmation of the particles and distribution, the elemental and mapping of the sample need to be done by the EDX and mapping analysis via SEM image. The result of EDX analysis is illustrated in Figure 2 (c). The result interprets the existence of five main elements in the sample; Ti, C, O, Pt and Ru. The detailed elemental discussion will be discussed in XRD and XPS results. Figure 2 (d) is the mapping analysis using the SEM image of PtRu/$Ti_3C_2T_x$ at magnification of 10 kX. The result shows that the small particle on top of the $Ti_3C_2T_x$ structure belongs to bimetal, Pt and Ru. Both metals are perceived well distributed on the MXene structure, indicating the appropriate and suitable parameter used during the reduction process. The even distribution of bimetal on the catalyst support structure can assist in the creation of an active reaction area during catalytic activity.

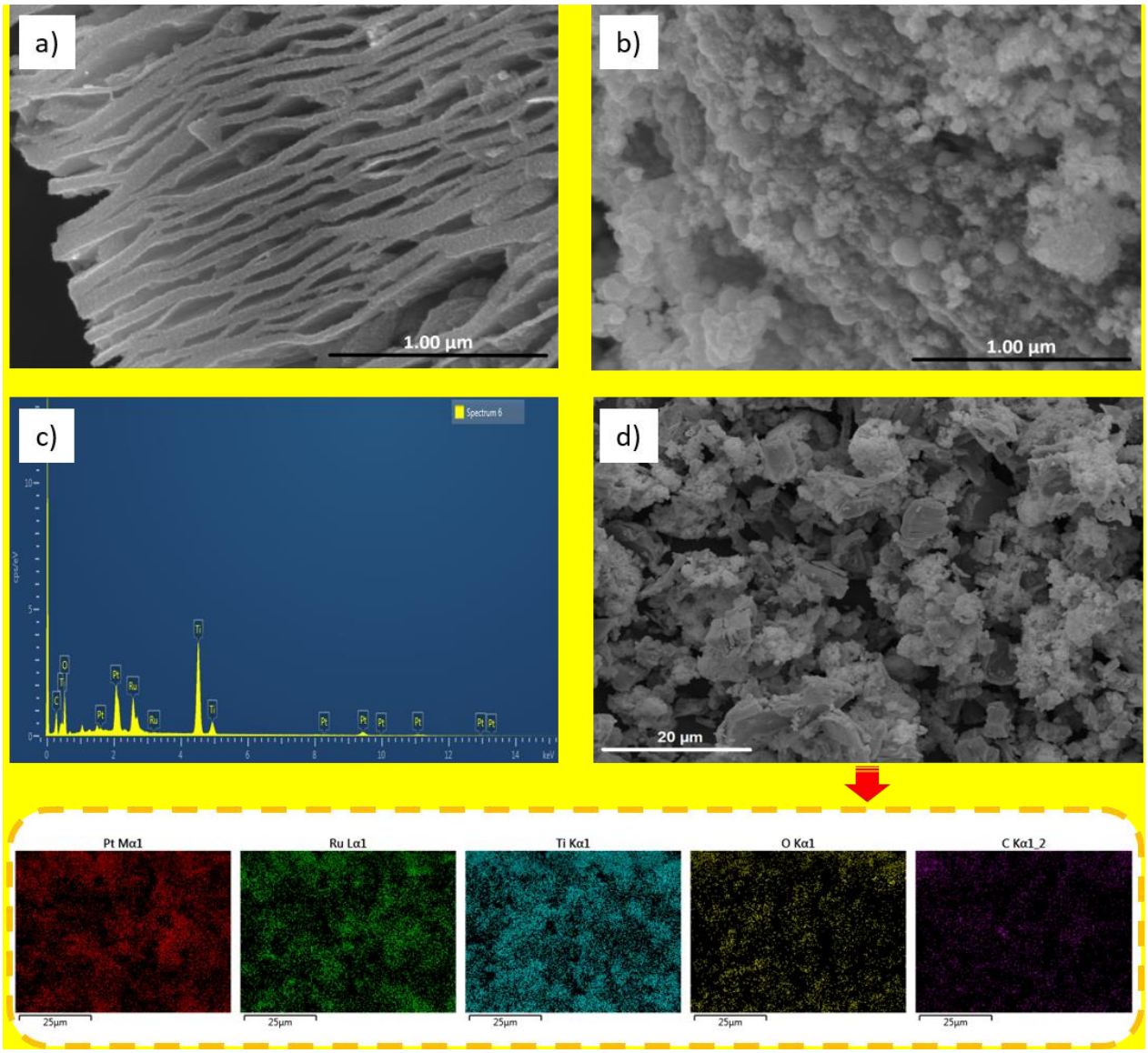

Figure 2: (a) FESEM image of $Ti_3C_2T_x$, (b) FESEM image of PtRu/$Ti_3C_2T_x$, (c) EDX of PtRu/$Ti_3C_2T_x$, and (d) SEM and mapping of PtRu/$Ti_3C_2T_x$

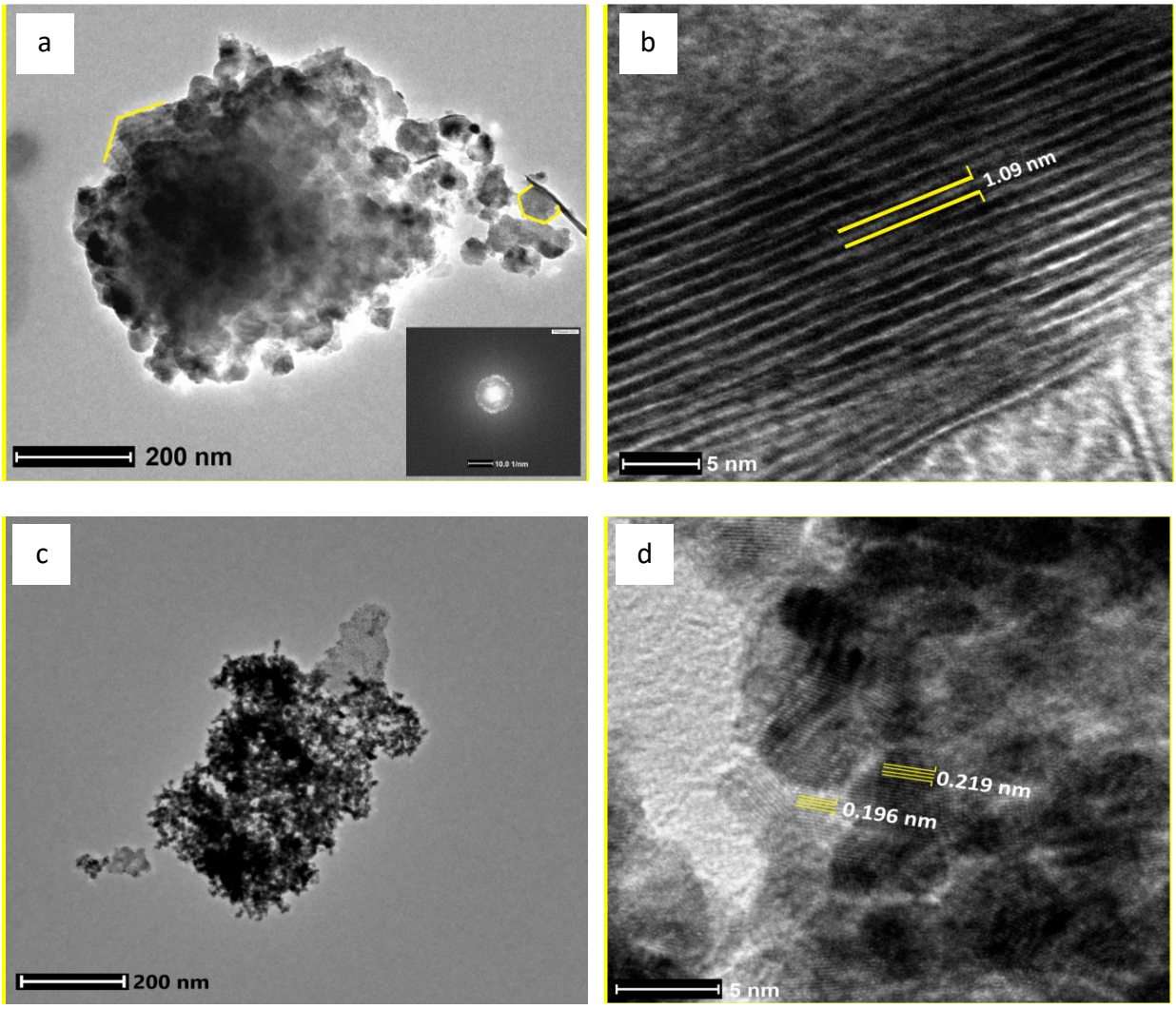

Figure 3: TEM image for, (a) and (b) $Ti_3C_2T_x$ catalyst support, (c) and (d) PtRu/$Ti_3C_2T_x$electrocatalyst

Further, the detailed morphology of the $Ti_3C_2T_x$ and PtRu/$Ti_3C_2T_x$ are studied using TEM for a low- and high-resolution image. A bundle of overlapping layered and flaky nanosheets can be seen clearly in Figure 3 (a) that corresponds to the $Ti_3C_2T_x$ structure. The overlapping image shown in Figure 3 (a) is the fast fourier transform (FFT) image, and it reveals the hexagonal-crystal structure, which is the feature of the MXene nanosheets [27]. Figure 3 (b) provides the image of a multilayer structure, nearly 20 layers, with an average interlayer spacing of 1.09 nm. Figure 3 (c)

and (d) is the TEM image for PtRu/$Ti_3C_2T_x$ electrocatalyst. The result shows that there is a cluster of Pt and Ru located on the surface of multilayer MXene and also in between the interlayer space, and the bimetal is seen to be well dispersed. The inner plane spacing of the bimetal is also measured and comes out with the average value of 0.219 nm and 0.196 nm for Pt and Ru nanoparticles.

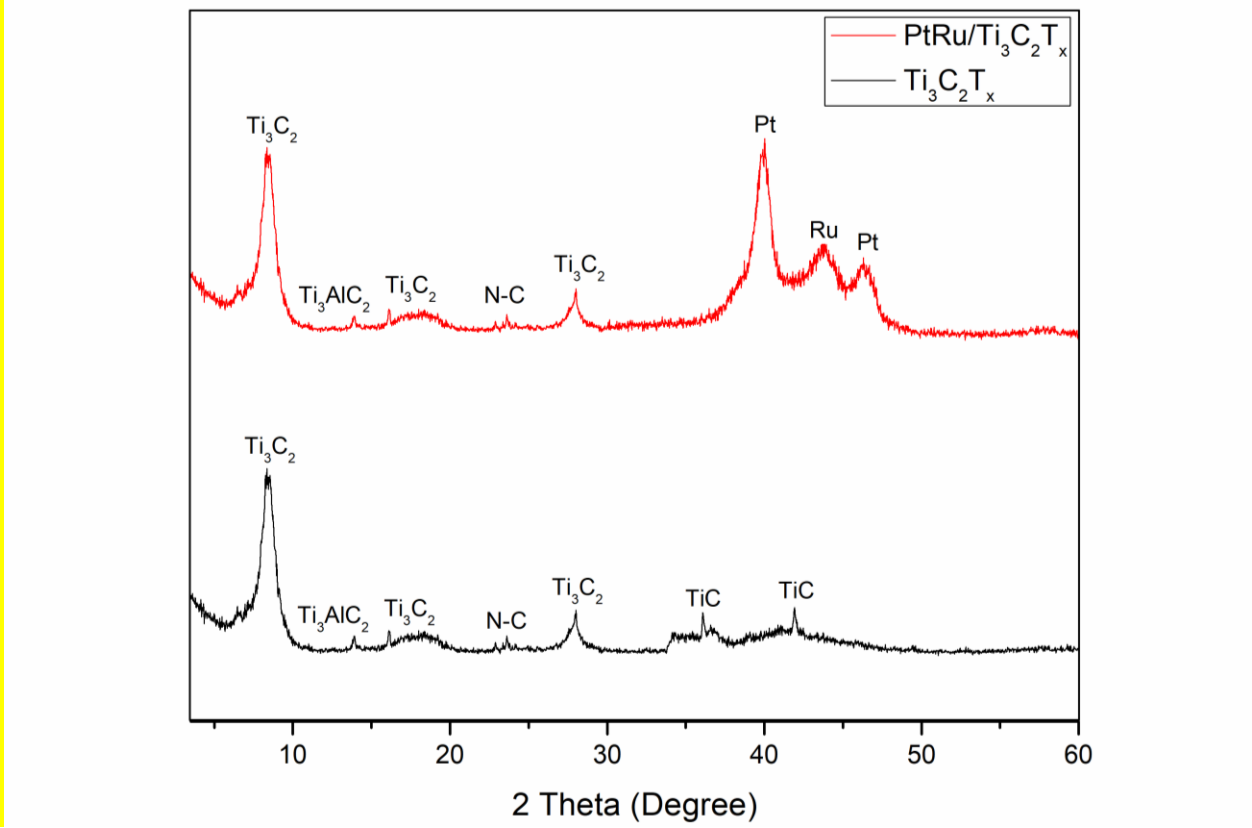

Figure 3: X-ray diffraction patterns for $Ti_3C_2T_x$ and PtRu/$Ti_3C_2T_x$

The elemental existence and crystallinity of $Ti_3C_2T_x$ catalyst support and PtRu/$Ti_3C_2T_x$ electrocatalyst are analyzed through XRD as shown in Figure 3. The material involved in the catalyst support, $Ti_3C_2T_x$, is featured in the sample and the diffraction peak is presented in the range of 3° to 60°. The pattern for $Ti_3C_2T_x$ catalyst support shows that the diffraction peak appeared at 8.5° (0 0 2), 18.6° (0 0 4) and 28° (0 0 6), where it reflected the existence of the Ti_3C_2 element. This result matches with the study carried out by Feng et al. [26] on a synthesis of MXene using

NH_4HF_2 as the etching agent. In addition, the small peaks at 24° (0 0 2) is belong to the nitrogen doped on the carbon element (N-C). Besides, there is the existence of small diffraction peak at 36° (1 1 1) and 41.8° (2 0 0), which is linked to the element of TiC, which is one of the elements in the MAX phase that have been used for $Ti_3C_2T_x$ preparation. The diffraction peak for the MAX phase used in the MXene synthesis, Ti_3AlC_2 can be seen around 13°, which is due to the incomplete etching process. However, the peak appeared is small and weak, while another peak for this MAX phase that should be at ~39° is completely disappeared. For PtRu/$Ti_3C_2T_x$ electrocatalyst sample, both peaks of Ti_3C_2 at 8.5° (0 0 1) and 28° (0 0 5) also appeared as is in the catalyst support sample. There is a presence of three new diffraction peaks for the electrocatalyst sample, which is 40° (1 1 1) and 46.2° (2 0 0) representing the Pt element, and 43.7° (1 0 1) for the Ru element. In addition, the crystallite sizes of the elements are gained from the numeric area or analytic peak profile analysis from XRD data by EVA software [28], which is quantified using the Debye-Scherrer equation as followed:

$$\text{Crystallite size(nm)} = 0.98\,\alpha\,/\,\beta\cos\theta \qquad \ldots\ldots. (1)$$

Where α, β and θ represent the X-ray wavelength, width of the peak at half-height and peak angle. The crystallite size for the Ti_3C_2, Pt and Ru elements are 9.17 nm, 10.14 nm and 17.4 nm, respectively. This XRD data verified the presence of Ti_3C_2, Pt and Ru elements in $Ti_3C_2T_x$ catalyst support and PtRu/$Ti_3C_2T_x$ electrocatalyst sample.

a)

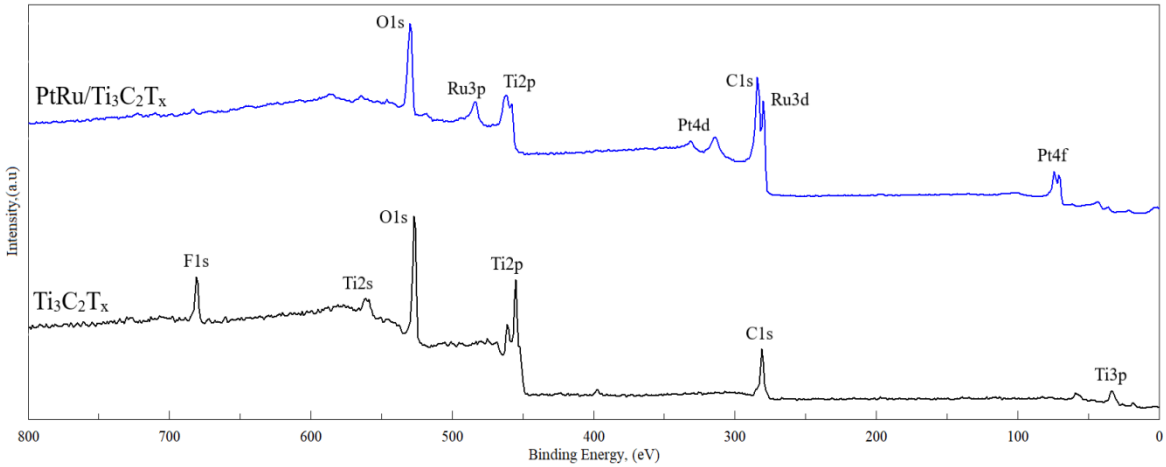
PtRu/Ti3C2Tx
O1s
Ru3p
Ti2p
C1s
Ru3d
Pt4d
Pt4f
Ti3C2Tx
F1s
Ti2s
O1s
Ti2p
C1s
Ti3p
Intensity,(a.u)
Binding Energy, (eV)

b)

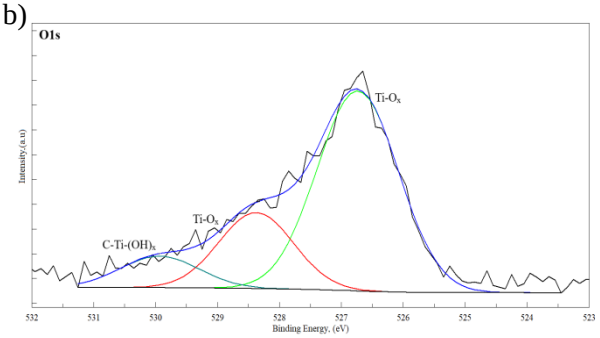
O1s
Ti-Ox
Ti-Ox
C-Ti-(OH)x
Intensity,(a.u)
Binding Energy, (eV)

f)

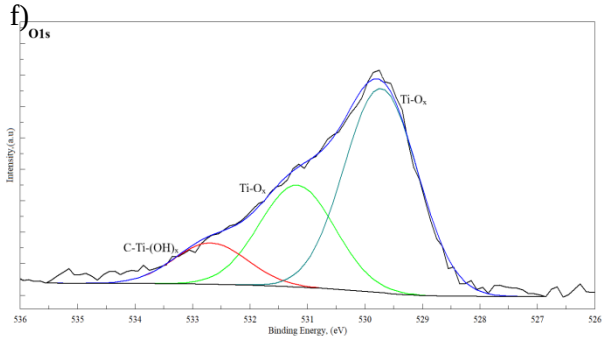
O1s
Ti-Ox
Ti-Ox
C-Ti-(OH)x
Binding Energy, (eV)

c)

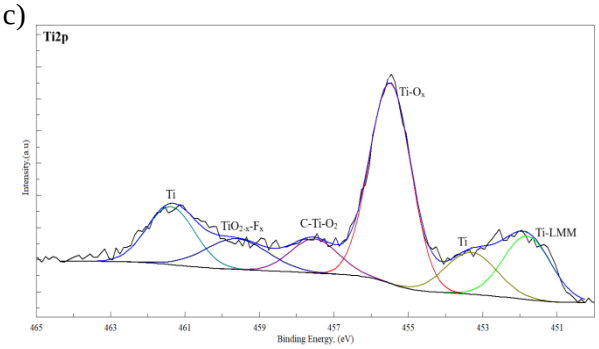
Ti2p
Ti-Ox
Ti
TiO2-xFx
C-Ti-O2
Ti
Ti-LMM
Intensity,(a.u)
Binding Energy, (eV)

g)

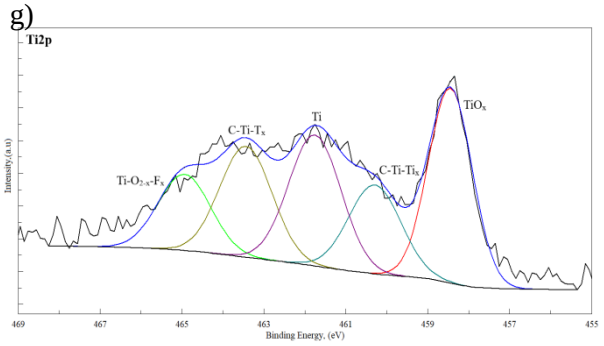
Ti2p
TiOx
C-Ti-Tx
Ti
Ti-O2-xFx
C-Ti-Tx
Binding Energy, (eV)

d)

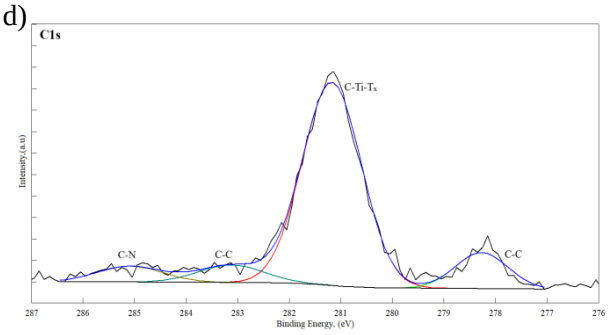
C1s
C-Ti-Tx
C-N
C-C
C-C
Intensity,(a.u)
Binding Energy, (eV)

h)

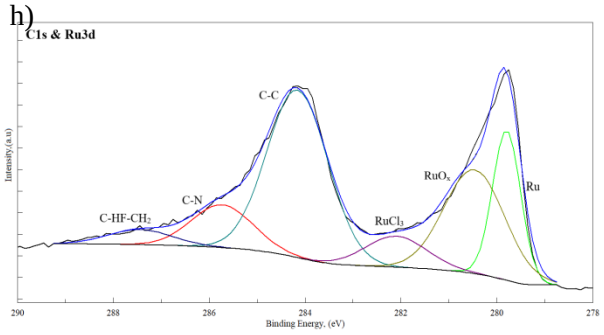
C1s & Ru3d
C-C
C-N
C-HF-CH2
RuOx
RuCl3
Ru
Intensity,(a.u)
Binding Energy, (eV)

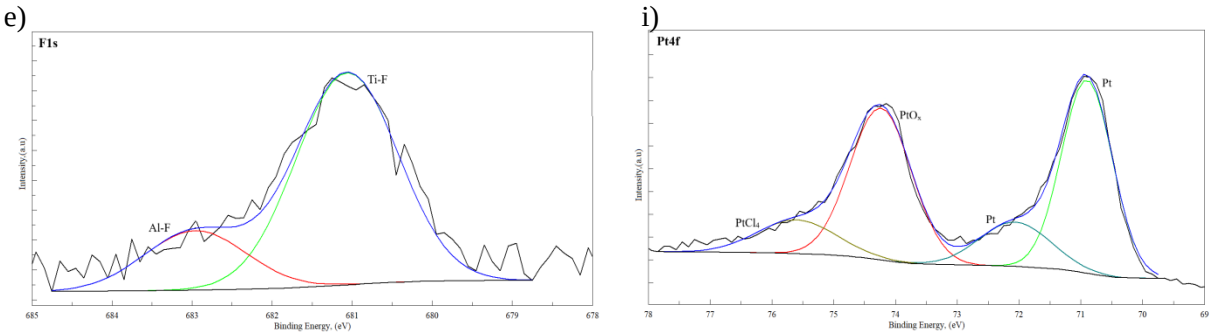

Figure 4: XPS analysis of (a) Survey spectra of $Ti_3C_2T_x$ and $PtRu/Ti_3C_2T_x$; High-resolution spectra of $Ti_3C_2T_x$ (b) O 1s, (c) Ti 2p, (d) C 1s, and (e) F 1s; High-resolution spectra of $PtRu/Ti_3C_2T_x$ (f) O 1s, (g) Ti 2p, (h) C 1s & Ru 3d, and (i) Pt 4f.

The XPS analysis was measured on $Ti_3C_2T_x$ and $PtRu/Ti_3C_2T_x$ to analyze the details of the material surface's chemistry. Figure 4 (a) is the survey spectra for both synthesis material, $Ti_3C_2T_x$ and $PtRu/Ti_3C_2T_x$, and the result shows that both spectra indicate the appearance of their element, which are O 1s, Ti 2p, C 1s and F 1s for $Ti_3C_2T_x$, while the element in $PtRu/Ti_3C_2T_x$ are O 1s, Ti 2p, C 1s, Pt 4f and Ru 3d. These entire elements agree with EDX and XRD analysis as stated before. The high-resolution spectra for $Ti_3C_2T_x$ (O 1s, Ti 2p, C 1s, F 1s) are shown in Figure 4 (b) – (e), while the high-resolution spectra for $PtRu/Ti_3C_2T_x$ (O 1s, Ti 2p, C 1s, Ru 3d and Pt 4f) is shown in Figure 4 (h) – (i). The result shows that most of the $Ti_3C_2T_x$ spectra overlapped with the $PtRu/Ti_3C_2T_x$ spectra, due to the same element used of $Ti_3C_2T_x$ in both samples. The high-resolution spectra for $Ti_3C_2T_x$ show that the O 1s spectra exhibit three peaks at 526.74 eV and 528.37 eV and 529.93 eV, which indicate the Ti-O_x and C-Ti-$(OH)_x$ bonds. Meanwhile, the Ti 2p spectra show six peaks at a binding energy of 451.81 eV, 453.30 eV and 461.38 eV, 455.48 eV, 457.52 eV, and 459.61 eV that corresponds to Ti-LMM, Ti, Ti-O_x, C-Ti-O_2, and TiO_{2-x}-F_x in MXene. The C 1s spectra exhibit the peaks at 278.27 eV and 283.12 eV, 281.17 eV, and 285.08 eV corresponding to C-C, C-Ti-T_x and C-N bond, whereas the additional F 1s spectra appear in

$Ti_3C_2T_x$ sample at a binding energy of 681.06 eV and 682.96 eV that may correspond to Ti-F and Al-F bond. The Ti 2P, O 1s, C 1s and F 1s spectrum have demonstrated the peaks corresponds to the $Ti_3C_2T_x$ sample with the formation of several termination groups like oxide (–O–), hydroxyl (–OH) and fluoride (–F). The nitrogen bonding also appeared in the sample due to the use of NH_4HF_2 as an etching agent, which may provide a good impact towards catalytic activity in MOR [29, 30].

The high-resolution spectra for PtRu/$Ti_3C_2T_x$ show that the O 1s and Ti 2p spectra indicate the same element as $Ti_3C_2T_x$. However, the high intensity peak of F 1s disappeared in the PtRu/$Ti_3C_2T_x$ sample; similar observation as studied by Zhao et al. [31] and Pan et al. [32]. This is due to the unstable F-termination that was replaced by the more stable metallic bonding of Pt and Ru during the chemical reduction process. The intensity of the peak C 1s also increased due to the appearance of Ru 3d element that is sharing the same binding energy range. The C 1s spectra exhibit three peaks at 284.1 eV, 285.73 eV and 287.44 eV that indicate the C-C, C-N and C-HF-CH_2 bonds, while another three peaks at 279.79 eV, 280.46 eV and 282.10 eV belong to Ru 3d spectra, which corresponds to Ru, RuO_2 and $RuCl_3$. The C-Ti-T_x bond as found in $Ti_3C_2T_x$ is cannot be found, which is due to the overlapping of a spectrum between C 1s and Ru 3d. The Pt 4f spectra show the appearance of four peaks at 70.9 eV and 72.07 eV indicating the metallic bond of Pt and 74.2 eV and 75.2 eV indicating the PtO and $PtCl_4$ bond. The $PtCl_4$ and $RuCl_3$ bond appeared due to the incomplete reduction process of metal precursor to metal during electrocatalyst synthesis. However, this bond is present in the weak peak and low intensity with below 10 % of the concentration percentage. Meanwhile, the formation of oxide (Ti-O_x, PtO and RuO_2) can be seen in both samples, which suggests the oxidation occurs during $Ti_3C_2T_x$ etching and PtRu/$Ti_3C_2T_x$ synthesis. The peaks of Al 2s and Al 2p supposedly around 1368 eV and 1414 eV

do not appear in both survey spectra indicating the successful etching process of Ti_3AlC_2 MAX phase to $Ti_3C_2T_x$ MXene. The binding energy for each peak is parallel with previous XPS studies by Kumar et al. [33], Shen et al. [34], Yang et al. [35], Kim et al. [36] and Chastain [37].

3.2 Electrochemical Measurement

Electrochemical measurements were performed to see the catalytic activity and potential of PtRu/$Ti_3C_2T_x$ as an anode electrocatalyst in DMFC. The main parameter for this section is the electrocatalyst loading between 0.35 to 0.55 $mgcm^{-2}$. The sample is annotated as PtRu/$Ti_3C_2T_x$ [electrocatalyst loading]. This parameter is one of the main parameters that affect catalytic activity [38-40]. The high electrocatalyst loading might expose more surface area and active catalytic sites for the MOR. However, the electrocatalyst loading has a certain optimum level in achieving the maximum catalytic activity. This performance involved five main electrochemical measurements, which are CV profile, LSV, CV curve, EIS and CA. Figure 5 shows the CV profile of an as-synthesized electrocatalyst in a 0.5 mol L^{-1} H_2SO_4 solution at a potential range of −0.2 to 1.0 V vs. Ag/AgCl and a scan rate of 20 mVs^{-1}. Through this profile, the ECSA is obtained in the hydrogen-adsorption region, which ranges from −0.2 to 0.1 V vs. Ag/AgCl. ECSA values are calculated using Eq. 2, as below:

$$\mathrm{ECSA}\ (\mathrm{m^2 g_{Pt}^{-1}}) = \mathrm{Q}/(\Gamma.\mathrm{W_{Pt}}) \qquad \ldots\ldots (2)$$

Where Q, Γ, and W_{Pt} are the charge density (the area under the graph for the hydrogen-adsorption region is divided by scan rate), the charge constant of the proton monolayer on the Pt, and the Pt loading [41], respectively.

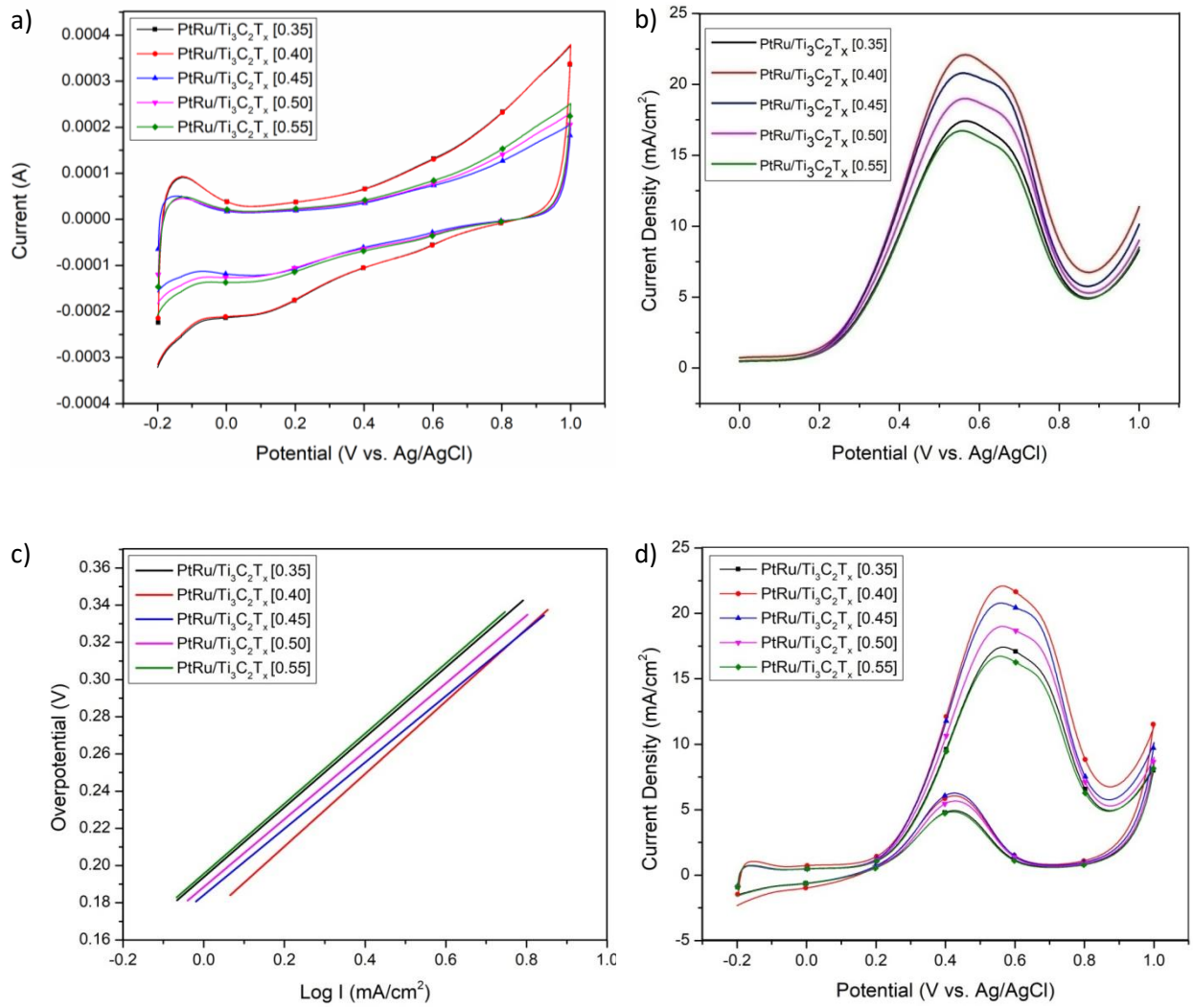

Figure 5: Electrochemical measurement of $PtRu/Ti_3C_2T_x$ samples; (a) CV profiles in 0.5 $molL^{-1}$ H_2SO_4 solution at a scan rate of 20 mVs^{-1}, (b) LSV curves in 2.8 $molL^{-1}$ CH_3OH and 0.5 $molL^{-1}$ H_2SO_4 solutions, (c) Tafel plots for all electrocatalysts with different loadings, (d) CV curves for all samples in 2.8 $molL^{-1}$ CH_3OH and 0.5 $molL^{-1}$ H_2SO_4 solution at a scan rate of 20 mVs^{-1}.

Table 1 shows the results for the CV profile and LSV analysis with different loading including the value of ECSA, Tafel slope, charge transfer coefficient and ion exchange current density. The ECSA results found that the $PtRu/Ti_3C_2T_x$ electrocatalyst with a loading of 0.40 $mgcm^{-2}$ has the highest electrochemical surface area with a value of 54.91 m^2g^{-1} followed by a

loading of 0.35, 0.45, 0.50 and 0.55 $mgcm^{-2}$. The trend of ECSA value can be seen clearly where it is in increasing order from 0.35 to 0.4 $mgcm^{-2}$, and subsequently decline for catalyst loading of 0.45 to 0.55 $mgcm^{-2}$. This indicate that catalyst loading of 0.4 $mgcm^{-2}$ has ability to provide more catalytically active sites on the electrode surface, thus leading to higher electrochemical activity. This result also indicates that the PtRu/$Ti_3C_2T_x$[0.40] electrocatalyst has the highest active area produced by Pt metal and is expected to maximize the surface active site for catalytic activity. Other than that, the high ECSA value also is due to the layered and flaky structures of MXene that assist the attachment of bimetal in more space and increased the active surface area for electrochemical performance. The higher catalyst loading of 0.45 to 0.55 $mgcm^{-2}$ facing lower ECSA value due to increased mass transport resistance, which causes the reduction of the potential active reaction surface area of the electrocatalyst and may lead to decreased the catalytic performance.

Table 1: Results of electrochemical measurement values with different loading

Electrocatalyst [Loading]	**ECSA ($m^2g_{Pt}^{-1}$)**	**Tafel slope, b ($mVdec^{-1}$)**	**Charge Transfer Coefficient, *α***	**Ion Exchange Current Density, *a* ($mA\ cm^{-2}$)**
PtRu/$Ti_3C_2T_x$ [0.35]	49.11	188	0.314	0.193
PtRu/$Ti_3C_2T_x$ [0.40]	54.91	196	0.301	0.170
PtRu/$Ti_3C_2T_x$ [0.45]	39.99	180	0.328	0.183
PtRu/$Ti_3C_2T_x$ [0.50]	28.74	184	0.321	0.188
PtRu/$Ti_3C_2T_x$ [0.55]	27.52	190	0.311	0.195

LSV is an electrochemical analysis that measures current response to voltage function. This analysis was performed in this study to identify the electron kinetic transfer, also known as Tafel analysis. The LSV curves of the electrocatalyst with different loading were plotted in Figure 5 (b),

where the current density measurement is normalized with geometric value. The curves were measured under an N_2 gas environment at a scan rate of 20 mVs^{-1} in the solution of 2.8 $molL^{-1}$ CH_3OH and 0.5 $molL^{-1}$ H_2SO_4. The curve is plotted in the range of potential 0.0 to 1.0 V vs. Ag/AgCl. The LSV result shows that the electrocatalyst with a loading of 0.40 $mgcm^{-2}$ exhibits the highest peak current density compared to other loadings. Eventhough the loading of the electrocatalyst is small, the current over an area is higher than other loadings, which indicates the capability of the electrocatalyst to maximize the reaction area and potential of the material to increase the overall MOR activity.

The LSV curve shows a significant increase in current density under the region between 0.18 – 0.35 V vs. Ag/AgCl, also known as the Tafel region. This active region occurs due to the electron kinetic transfer that occurs between the surface of the electrocatalyst and the electrode. The extraction results from the region are plotted and known as the Tafel plot. The region is extracted using Eq. (4) and (5) as below [42]:

$$\eta = a + b \log\ (i) \qquad \ldots\ldots (4)$$

$$b = 2.3RT/\alpha F \qquad \ldots\ldots (5)$$

Where η and I are overpotentials and current density in the Tafel region, meanwhile a and b represent ion exchange current density and Tafel slope, respectively. For Eq. 5, R is a gas constant, T is a temperature, F is a Faraday constant and α is the charge transfer coefficient. Figure 5 (c) shows the Tafel plot for all the electrocatalysts with different loadings. Meanwhile, the overall data of the Tafel plots are tabulated in Table 1.

Tafel plot results show that the Tafel slope is around 180 to 196 $mVdec^{-1}$, and it is within the value for the methanol decomposition process on Pt surfaces, which is around 95 – 440 $mVdec^{-1}$, based on a different type of Pt group [43]. The closest Pt group with the Tafel slope value for

the as-synthesized electrocatalyst is the polycrystalline (pc)-Pt group with 200 $mVdec^{-1}$. The measured Tafel slope is near the theoretical value which indicates that there is the MOR occurs with the first electron transfer from the split of the C-H bond of methanol molecules [44]. The higher the Tafel slope, the slower the reaction activity because of the formation of the CO_{ad}. The slope for the formation of the CO_{ad} in the methanol reaction is estimated to be 440 $\pm$ 30 $mVdec^{-1}$ [45] and the measured Tafel slope for $PtRu/Ti_3C_2T_x$ electrocatalyst is very much smaller, which is within 180 – 196 $mVdec^{-1}$. Therefore, this electrocatalyst has good resistance towards the formation of CO, hence potentially reducing the catalyst poisoning.

The charge transfer coefficient, α, for the $PtRu/Ti_3C_2T_x$ electrocatalyst is around 0.3 $\pm$ 0.028. This measured coefficient agrees with other studies [43] that indicate the α value of C-H bond breaking. This considered that there are the MOR occurs at the forward scan of electrochemical analysis; hence proving the potential of the as-synthesized electrocatalyst in MOR activity. At the same time, *a* value did not show a significant difference between electrocatalysts which lies in the range of 0.170 – 0.195 $mAcm^{-2}$. This indicates that the electrocatalyst loading does not significantly affect the decomposition of catalytic activity. This result also demonstrates that the electrocatalyst that undergoes the combination of bimetallic and 2D structure material can produce catalytic activity decomposition, thus potentially emerging as one of the promising electrocatalysts for MOR in DMFC application.

Table 2: Result of CV curve analysis

Electrocatalyst	**Onset Potential (V vs. Ag/AgCl)**	**Peak Potential (V vs. Ag/AgCl)**	**Current Density ($mAcm^{-2}$)**	**I_f/I_b Ratio**
$PtRu/Ti_3C_2T_x$ [0.35]	0.268	0.566	17.418	3.53
$PtRu/Ti_3C_2T_x$ [0.40]	0.259	0.564	22.093	3.64
$PtRu/Ti_3C_2T_x$ [0.45]	0.266	0.560	20.792	3.31

PtRu/$Ti_3C_2T_x$ [0.50]	0.266	0.562	19.001	3.35
PtRu/$Ti_3C_2T_x$ [0.55]	0.276	0.556	16.721	3.46

Figure 5 (d) is the CV curve for all the different loading of the electrocatalyst. This curve can measure the level of catalytic activity occurring on the PtRu/$Ti_3C_2T_x$ electrocatalysts. All CV curves were measured in 2.8 $molL^{-1}$ CH_3OH solution with 0.5 $molL^{-1}$ H_2SO_4 at room temperature with oxygen-free content. The ranges of potential for all curves were obtained from −0.2 to 1 V vs. Ag/AgCl. The result for the CV curve is tabulated in Table 2. The results show that the peak current density increases as the electrocatalyst loading increases. However, the peak current density value reached the highest value at a loading of 0.40 $mgcm^{-2}$, and then it began to decline as loading increased. The trend of CV results is in line with the ECSA value. This indicates that the active surface reaction area contributes to the electrocatalytic activity in the methanol oxidation reaction, where a high electrochemical surface area leads to the appearance of catalytic reaction hot spots.This is also driven by the good distribution of PtRu metal on the $Ti_3C_2T_x$ catalyst support surface as illustrated in the SEM results. This uniform distribution can expose more active PtRu metal sites and lead to stronger interactions between metal-catalyst supports, leading to maximum methanol adsorption.

In addition, this CV curve also provides the onset potential values for each of the different electrocatalyst loadings as scheduled in Table 1. The results show that the onset potential of the loading of 0.40 (0.259 V vs. Ag/AgCl) is the most negative when compared to the other loadings. The negatively charged value is better because it indicates the simple removal of intermediate CO adsorbed on the electrocatalyst surface resulting from strong OH adsorption. This is because of the presence of catalyst support, $Ti_3C_2T_x$, which has a superior Ti material with oxophilic properties. This property can tune the electronic structure of the metal and provide more oxophilic

sites, where it can weaken CO adsorption and enhance OH adsorption [46]. This simple removal of the intermediate CO influences the catalytic activity, where the more negative value of onset potential, the higher the catalytic activity recorded towards MOR. Similar results were reported by Lu et al. [46], Liu et al. [44], and Zhu et al [47].

Figure 5 (d) also shows the appearance of the reverse oxidation peak in the CV curve. This peak occurs due to the incomplete formation of carbonated species that involve the presence of CO at the forward oxidation peak which is the major cause of electrocatalyst poisoning. The ratio of the forward (I_f) and reverse (I_b) oxidation peaks also known as CO tolerance was evaluated and found that a loading of 0.40 had the highest value of 3.64. This indicates that the electrocatalyst loading of 0.40 has good tolerance to CO species, which automatically portrays a low level of poisoning. However, CO tolerance values for other loadings were also high, ranging from 3.31 to 3.64, indicating that the PtRu metal and 2D $Ti_3C_2T_x$ combination has a high potential in reducing catalyst poisoning problems which are among the major problems in DMFC.

Table 3: Comparison between commercial and 2D structure electrocatalysts for MOR activity

Authors	**Electro-catalysts**	**ECSA ($m^2g_{Pt}^{-1}$)**	**Peak Potential (V vs Ag/AgCl)**	**Geometric Current Density ($mAcm^{-2}$)**	**ECSA Current Density ($mAcm_{ECSA}^{-2}$)**
This study	$PtRu/Ti_3C_2T_x$	54.9	0.56	22.09	1.19
Ramirez et al. [48]	Pt/C	6.42	0.69	4.30	-
Wang et al. [49]	PtRu/C	49.0	-	-	0.83
Wang et al. [22]	Pt/ $Ti_3C_2T_x$	30.2	0.68	1.14	-
Zhai et al. [50]	Pt-MoS_2/rGO	12.9	0.74	7.35	-
Patil et al. [51]	Pt/GNS	13.0	0.37	2.61	-
Shahrokhian et al. [52]	PtPd-NPs/ rGO	-	0.74	-	0.62
Sha et al. [53]	Pt NFs-rGO	-	0.78	15.30	-

Kumar et al. [54]	Pt/rGO	-	0.60	-	0.42

Table 3 shows the results of a comparison of the as-synthesized electrocatalyst, PtRu/$Ti_3C_2T_x$ with several commercial electrocatalysts, Pt-based and 2D structured materials electrocatalyst for MOR activity, in acidic media. All these electrocatalysts were compared to the ECSA value, geometric and ECSA normalized current density as well as peak potential. The comparative results show that the PtRu/$Ti_3C_2T_x$ electrocatalyst exhibits the highest geometric current density compared to other electrocatalysts, which is about 5.13 times more than the Pt/C commercial electrocatalyst. This is aided by the natural structure of MXene which opens up a more active spot on the surface, thus enhancing the active reaction site of this composite electrocatalyst. Besides, the comparison of geometric current density between PtRu/$Ti_3C_2T_x$ and Pt/$Ti_3C_2T_x$ shows that the as-synthesized electrocatalyst has a much higher value. This finding is like several other studies that found the use of PtRu bimetallic had a better performance than the use of Pt single component [41, 55]. This is due to the presence of Ru metal which plays a role in reducing the bonding strength of CO and resulting in weak CO adsorption, thus reducing catalytic poisoning and improving electrocatalytic performance [41]. However, the individual contribution of each component of the material cannot be thoroughly analyzed, and further investigation is highly recommended to better understand the synergistic effect and its impact on catalytic performance. In addition to geometric current density, the ECSA normalized current density also show the high value of as-synthesized electrocatalyst compared with other study. This suggests that the PtRu/$Ti_3C_2T_x$ has a higher intrinsic activity compared with other Pt-based electrocatalyst, indicating that there are more exposed catalytically active sites and better mass transport during the MOR [56]. The comparison of peak potential value with other electrocatalysts is also evaluated. Generally, the PtRu/$Ti_3C_2T_x$ electrocatalyst is placed in the third list of more negative

peak potential values. A more negative peak potential value is better, indicating that this electrocatalyst has significant potential in CO resistance [57].

The EIS measurement is analyzed to identify the associated phenomena that occur on the interface of electrocatalyst material during MOR. The measurement is conducted in the solution of 2.8 $molL^{-1}$ CH_3OH and 0.5 $molL^{-1}$ H_2SO_4 at a frequency range between 100 kHz and 1 Hz. Figure 6 (a) shows the Nyquist plot for PtRu/$Ti_3C_2T_x$ electrocatalyst with different loading. The plot for all samples displays the same pattern; where there is a small semicircle shape linked with the straight line. The semicircle diameter corresponds to the electron transfer kinetics between the solution and electrode interface and charge-transfer resistance (R_{ct}). Meanwhile, the straight line is related to the ion diffusion at the electrode interface from the bulk solution, which represents the Warburg impedance. The Nyquist plots were fitted using the modified Randles equivalent circuit model illustrated in Figure 6 (b). The circuit consists of two resistors (R_s and R_{ct}) that correspond to the resistance of bulk solution and charge transfer resistance, Warburg element (W), capacitance and constant phase element (CPE). The EIS result shows that the loading of 0.4 PtRu/$Ti_3C_2T_x$ electrocatalyst exhibits the smallest diameter of a semicircle, representing the lowest charge-transfer resistance among all samples. This is due to the rapid transport of carried charge that can be achieved due to the better conductivity and higher surface area of electrocatalyst material, leading to the facile methanol oxidation reaction [58]. In addition, the low charge-transfer resistance also can increase the efficiency of the methanol absorption in the catalyst interface; improving the electrocatalytic activity which explained the high activity of this sample in the CV results. The equivalent circuit model has included a Warburg element in series with a charge transfer resistance. This arrangement describes the diffusion of electroactive species to the

electrode surface in this reaction, where they undergo the oxidation reaction via charge transfer [59]. This is proved that the reaction proceeds through diffusion-controlled phenomena.

a)

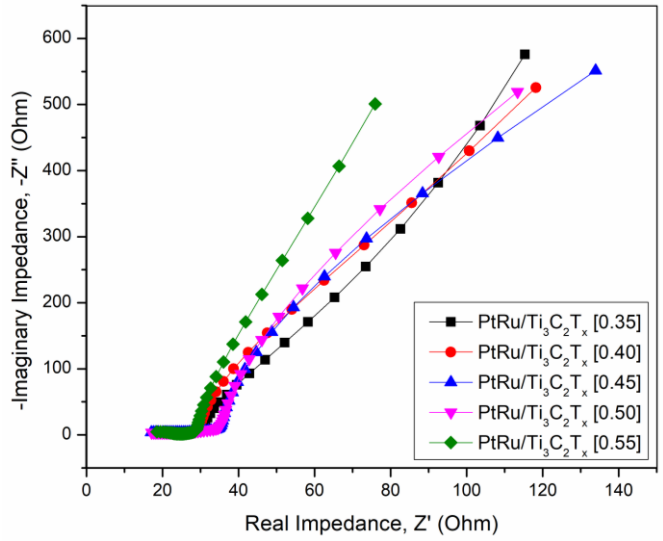

b)

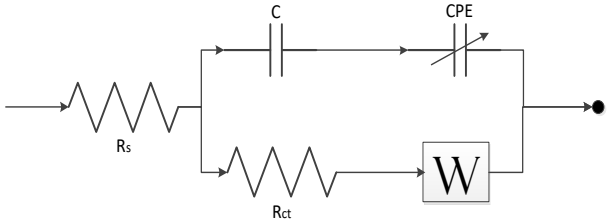

c)

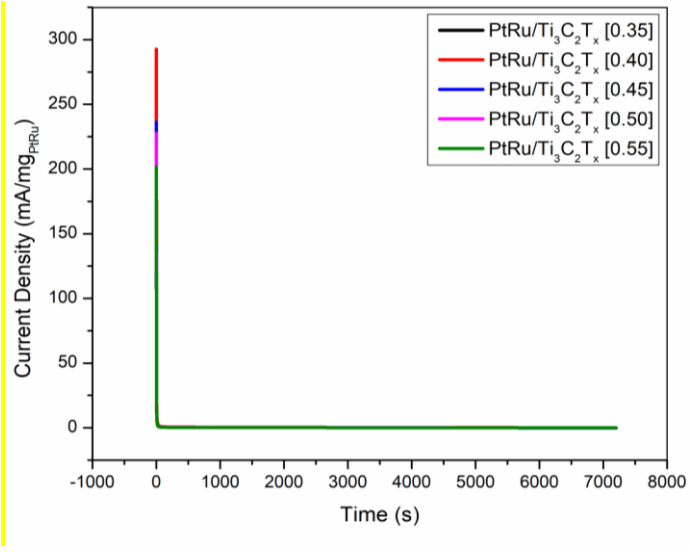

Figure 6: Electrochemical measurement of $PtRu/Ti_3C_2T_x$ with different catalyst loading in 2.8 $molL^{-1}$ CH_3OH and 0.5 $molL^{-1}$ H_2SO_4 solutions; (a) Nyquist plot and (b) Equivalent electrical

circuit for EIS measurement of half-cell performance; (c) CA curves at the potential of 0.5 V vs. Ag/AgCl for 7200s.

In addition to CV and EIS study, CA analysis was also performed on the PtRu/$Ti_3C_2T_x$ to see the stability of the electrocatalyst. This analysis was carried out for 7200 s in 2.8 $molL^{-1}$ CH_3OH and 0.5 $molL^{-1}$ H_2SO_4 solution at a constant potential of 0.5 V vs. Ag/AgCl as shown in Figure 6 (c). The results show that all the electrocatalyst loadings produced a sudden decline at the beginning of the analysis due to the poisoning effect from intermediate species of methanol oxidation. This trend indicates that the loading factor does not significantly affect the stability of the electrocatalyst. After 900 s, all the studied electrocatalysts exhibit a relatively steady-state behavior. However, loading of 0.4 $mgcm^{-2}$ produced the highest current density after 7200 s compared to the other electrocatalyst loadings. This is due to the good dispersion of PtRu and MXene on the active electrode area and able to maximize the catalytic activity. The high current density over a long period also indicates the superiority of MOR kinetics by using PtRu/$Ti_3C_2T_x$ as an electrocatalyst.

The electrocatalyst loading of 0.4 $mgcm^{-2}$ for PtRu/$Ti_3C_2T_x$ demonstrated the highest electrochemical surface area, catalytic activity, catalyst poisoning resistance, low charge-transfer resistance, and better stability, making it the optimal loading for MOR performance. These findings highlight the significance of the electrocatalyst loading in enhancing catalytic activity for MOR. Additionally, the use of $Ti_3C_2T_x$ as a catalyst support and the presence of bimetallic Pt and Ru have shown promising results in increasing catalytic activity, making them a viable substitute for commercial electrocatalysts in DMFC applications. These findings are significant in advancing the development of multifunctional nanomaterials for more efficient and reliable sources of

affordable and clean energy, contributing to the advancement of future promising green power sources technology.

4. CONCLUSIONS

The PtRu/$Ti_3C_2T_x$ electrocatalyst was synthesized using the chemical reduction method and applied as an electrocatalyst for MOR. The different electrocatalyst loading, ranging between 0.35 to 0.55 $mgcm^{-2}$, were prepared to compare the effect on the catalytic activity in MOR. The physical characterization proved that the PtRu/$Ti_3C_2T_x$ electrocatalyst was successfully synthesized when all the elements (Ti_3C_2, Pt and Ru) exist in the samples that come out with a small crystallite size of below 18 nm. The XPS analysis demonstrates the appearance of termination groups of –O, –OH, and –N in the $Ti_3C_2T_x$ sample, as well as metallic Pt and Ru in PtRu/$Ti_3C_2T_x$. The morphology of the samples portrays the layered and flaky structure of MXene with well-distributed Pt and Ru on the MXene. The electrochemical measurements reveal that the electrocatalyst loading of 0.40 $mgcm^{-2}$ exhibits the highest ECSA and peak current density value of 22.09 $mAcm^{-2}$, as well as better tolerance towards catalyst poisoning and the smallest charge-transfer resistance. The comparison with the previous study shows that the PtRu/$Ti_3C_2T_x$ electrocatalyst exhibits the highest catalytic activity, which is about 5.13 times more than the Pt/C commercial electrocatalyst. Thus, the incorporation of $Ti_3C_2T_x$ with Pt and Ru has been observed to enhance the catalytic activity and can serve as a potential alternative to commercial anode electrocatalysts in DMFC applications. This study's findings hold great importance in the progress of multifunctional nanomaterials for the creation of efficient, reliable, and affordable energy sources, contributing towards the advancement of future green power technologies.

ACKNOWLEDGEMENT

The authors would like to acknowledge the financial support provided by Sunway University through project no #STR-RCGS-MATSCI[S]-001-2021.

REFERENCES

1. Kumar, A., et al., *A review of multi criteria decision making (MCDM) towards sustainable renewable energy development.* Renewable Sustainable Energy Reviews, 2017. **69**: p. 596-609.
2. Fernando, Y., W.X. Wah, and M.S. Shaharudin, *Does a firm's innovation category matter in practising eco-innovation? Evidence from the lens of Malaysia companies practicing green technology.* Journal of Manufacturing Technology Management, 2016.
3. Zhao, X., et al., *High-temperature passive direct methanol fuel cells operating with concentrated fuels.* Journal of Power Sources, 2015. **273**: p. 517-521.
4. Kamarudin, S.K., et al., *Overview on the challenges and developments of micro-direct methanol fuel cells (DMFC).* Journal of power sources, 2007. **163**(2): p. 743-754.
5. Abdullah, N., et al., *Synthesis and optimization of PtRu/TiO2-CNF anodic catalyst for direct methanol fuel cell.* International Journal of Hydrogen Energy, 2019. **44**(58): p. 30543-30552.
6. Mansor, M., et al., *Recent progress of anode catalysts and their support materials for methanol electrooxidation reaction.* International Journal of Hydrogen Energy, 2019. **44**(29): p. 14744-14769.
7. Yang, Z., et al., *An Enhanced Anode based on Polymer-Coated Carbon Black for use as a Direct Methanol Fuel Cell Electrocatalyst.* ChemCatChem, 2015. **7**(5): p. 808-813.
8. Anitha, V., et al., *Anodic TiO2 nanotubes decorated by Pt nanoparticles using ALD: An efficient electrocatalyst for methanol oxidation.* Journal of Catalysis, 2018. **365**: p. 86-93.
9. Xie, F., et al., *One-pot construction of the carbon spheres embellished by layered double hydroxide with abundant hydroxyl groups for Pt-based catalyst support in methanol electrooxidation.* Journal of Power Sources, 2019. **420**: p. 73-81.

10. Abdullah, M., S.K. Kamarudin, and L. Shyuan, *TiO 2 Nanotube-Carbon (TNT-C) as Support for Pt-based Catalyst for High Methanol Oxidation Reaction in Direct Methanol Fuel Cell.* Nanoscale research letters, 2016. **11**(1): p. 553.
11. Abdullah, N., et al., *Fabrication and Characterization of New Composite Tio 2 Carbon Nanofiber Anodic Catalyst Support for Direct Methanol Fuel Cell via Electrospinning Method.* Nanoscale research letters, 2017. **12**(1): p. 613.
12. Chen, X., et al., *Multi-component nanoporous platinum–ruthenium–copper–osmium–iridium alloy with enhanced electrocatalytic activity towards methanol oxidation and oxygen reduction.* Journal of Power Sources, 2015. **273**: p. 324-332.
13. Ramli, Z.A.C., et al., *Synthesis, Characterization and Potential of Pt-Ru Supported Carbon Nanocage (CNC) for Methanol Oxidation Reaction (MOR) and DMFC Application.* International Journal of Integrated Engineering, 2019. **11**(7): p. 190-200.
14. Abraham, B.G., R. Bhaskaran, and R. Chetty, *Electrodeposited bimetallic (PtPd, PtRu, PtSn) catalysts on titanium support for methanol oxidation in direct methanol fuel cells.* Journal of The Electrochemical Society, 2020. **167**(2): p. 024512.
15. Dong, K., et al., *Dendric nanoarchitectonics of PtRu alloy catalysts for ethylene glycol oxidation and methanol oxidation reactions.* Journal of Alloys Compounds, 2022. **905**: p. 164231.
16. Luo, B., et al., *Facile synthesis of PtRu nanodendrites/graphene catalyst with excellent performance for methanol oxidation.* Materials Letters, 2022. **308**: p. 131145.
17. Sekar, A., et al., *PtRu catalysts on nitrogen-doped carbon nanotubes with conformal hydrogenated TiO2 shells for methanol oxidation.* ACS Applied Nano Materials, 2022. **5**(3): p. 3275-3288.
18. Sharma, S. and B.G. Pollet, *Support materials for PEMFC and DMFC electrocatalysts—a review.* Journal of Power Sources, 2012. **208**: p. 96-119.
19. Basri, S., et al., *Nanocatalyst for direct methanol fuel cell (DMFC).* International Journal of Hydrogen Energy, 2010. **35**(15): p. 7957-7970.
20. Yuan, W. and L. Cheng, *MXenes for Electrocatalysis.* MXenes: Fundamentals Applications, 2019. **51**: p. 74-104.

21. Aslfattahi, N., et al., *MXene based new class of silicone oil nanofluids for the performance improvement of concentrated photovoltaic thermal collector.* Solar Energy Materials and Solar Cells, 2020. **211**: p. 110526.
22. Wang, Y., et al., *Pt decorated Ti3C2 MXene for enhanced methanol oxidation reaction.* Ceramics International, 2019. **45**(2): p. 2411-2417.
23. Zhang, X., et al., *Preparation of Pt/(Ti3C2Tx) y-(MWCNTs) 1-y electrocatalysts via a facile and scalable solvothermal strategy for high-efficiency methanol oxidation.* Applied Catalysis A: General, 2019. **585**: p. 117181.
24. Aslfattahi, N., et al., *Experimental investigation of energy storage properties and thermal conductivity of a novel organic phase change material/MXene as A new class of nanocomposites.* Journal of Energy Storage, 2020. **27**: p. 101115.
25. Abdullah, N., et al., *Optimization of electrocatalyst performance of platinum–ruthenium induced with MXene by response surface methodology for clean energy application.* Journal of Cleaner Production, 2020. **277**: p. 123395.
26. Feng, A., et al., *Fabrication and thermal stability of NH4HF2-etched Ti3C2 MXene.* Ceramics International, 2017. **43**(8): p. 6322-6328.
27. Kong, F., et al., *Improving the electrochemical properties of MXene Ti3C2 multilayer for Li-ion batteries by vacuum calcination.* Electrochimica Acta, 2018. **265**: p. 140-150.
28. Bruker. *Diffrac.eva*. X-Ray Diffraction (XRD) 2022 [cited 2022 30 August].
29. Tan, Q., et al., *Highly dispersed Pd-CeO2 nanoparticles supported on N-doped core–shell structured mesoporous carbon for methanol oxidation in alkaline media.* ACS Catalysis, 2019. **9**(7): p. 6362-6371.
30. Zhang, K., et al., *Multi-dimensional Pt/Ni (OH) 2/nitrogen-doped graphene nanocomposites with low platinum content for methanol oxidation reaction with highly catalytic performance.* Chemical Engineering Journal, 2021. **421**: p. 127786.
31. Zhao, D., et al., *Alkali-induced 3D crinkled porous Ti 3 C 2 MXene architectures coupled with NiCoP bimetallic phosphide nanoparticles as anodes for high-performance sodium-ion batteries.* Energy Environmental Science, 2019. **12**(8): p. 2422-2432.
32. Pan, Z. and X. Ji, *Facile synthesis of nitrogen and oxygen co-doped C@ Ti3C2 MXene for high performance symmetric supercapacitors.* Journal of Power Sources, 2019. **439**: p. 227068.

33. Kumar, A., et al., *Influence of different parameters on total fluoride concentration evaluation in ex-situ chemical degradation of nafion based membrane.* Korean Journal of Chemical Engineering, 2021. **38**(10): p. 2057-2063.
34. Shen, B., et al., *Bottom-up construction of three-dimensional porous MXene/nitrogen-doped graphene architectures as efficient hydrogen evolution electrocatalysts.* International Journal of Hydrogen Energy, 2021. **46**(58): p. 29984-29993.
35. Yang, C., et al., *Pd nanocrystals grown on MXene and reduced graphene oxide co-constructed three-dimensional nanoarchitectures for efficient formic acid oxidation reaction.* International Journal of Hydrogen Energy, 2021. **46**(1): p. 589-598.
36. Kim, H.J., et al., *Highly active and stable PtRuSn/C catalyst for electrooxidations of ethylene glycol and glycerol.* Applied Catalysis B: Environmental, 2011. **101**(3-4): p. 366-375.
37. Chastain, J. and R.C. King Jr, *Handbook of X-ray photoelectron spectroscopy.* Perkin-Elmer Corporation, 1992. **40**: p. 221.
38. Abukhadra, M.R., et al., *Synthesis of Na+ trapped bentonite/zeolite-P composite as a novel catalyst for effective production of biodiesel from palm oil; Effect of ultrasonic irradiation and mechanism.* Energy Conversion Management, 2019. **196**: p. 739-750.
39. Li, S. and L. Guo, *Stability and activity of a co-precipitated Mg promoted Ni/Al2O3 catalyst for supercritical water gasification of biomass.* International Journal of Hydrogen Energy, 2019. **44**(30): p. 15842-15852.
40. Park, J.C. and C.H. Choi, *Graphene-derived Fe/Co-NC catalyst in direct methanol fuel cells: Effects of the methanol concentration and ionomer content on cell performance.* Journal of power sources, 2017. **358**: p. 76-84.
41. Abdullah, N., S.K. Kamarudin, and L. Shyuan, *Novel anodic catalyst support for direct methanol fuel cell: characterizations and single-cell performances.* Nanoscale research letters, 2018. **13**(1): p. 90.
42. Askari, M.B., et al., *Fe3O4@ MoS2/RGO as an effective nano-electrocatalyst toward electrochemical hydrogen evolution reaction and methanol oxidation in two settings for fuel cell application.* Journal of colloid interface science, 2019. **537**: p. 186-196.
43. Fang, Y.-H. and Z.-P. Liu, *First principles Tafel kinetics of methanol oxidation on Pt (111).* Surface Science, 2015. **631**: p. 42-47.

44. Liu, G., et al., *A novel TiN coated CNTs nanocomposite CNTs@ TiN supported Pt electrocatalyst with enhanced catalytic activity and durability for methanol oxidation reaction.* International Journal of Hydrogen Energy, 2017. **42**(17): p. 12467-12476.
45. Liu, S.X., et al., *The kinetics of CO pathway in methanol oxidation at Pt electrodes, a quantitative study by ATR-FTIR spectroscopy.* Physical Chemistry Chemical Physics, 2011. **13**(20): p. 9725-9735.
46. Lu, S., et al., *Promoting the methanol oxidation catalytic activity by introducing surface nickel on platinum nanoparticles.* Nano Research, 2018. **11**(4): p. 2058-2068.
47. Zhu, J., G. He, and P.K. Shen, *A cobalt phosphide on carbon decorated Pt catalyst with excellent electrocatalytic performance for direct methanol oxidation.* Journal of power sources, 2015. **275**: p. 279-283.
48. Ramirez, A.M., et al., *Effect of different zeolite as Pt supports for methanol oxidation reaction.* Applied Surface Science, 2018. **456**: p. 204-214.
49. Wang, Q., et al., *Surface Ru enriched structurally ordered intermetallic PtFe@ PtRuFe core-shell nanostructure boosts methanol oxidation reaction catalysis.* Applied Catalysis B: Environmental, 2019. **252**: p. 120-127.
50. Zhai, C., et al., *Two dimensional MoS2/graphene composites as promising supports for Pt electrocatalysts towards methanol oxidation.* Journal of Power Sources, 2015. **275**: p. 483-488.
51. Patil, S.H., et al., *Architecturally designed Pt–MoS 2 and Pt–graphene composites for electrocatalytic methanol oxidation.* Physical Chemistry Chemical Physics, 2015. **17**(39): p. 26101-26110.
52. Shahrokhian, S. and S. Rezaee, *Vertically standing Cu2O nanosheets promoted flower-like PtPd nanostructures supported on reduced graphene oxide for methanol electro-oxidation.* Electrochimica Acta, 2018. **259**: p. 36-47.
53. Sha, R. and S. Badhulika, *Facile synthesis of three-dimensional platinum nanoflowers decorated reduced graphene oxide: An ultra-high performance electro-catalyst for direct methanol fuel cells.* Materials Science Engineering: B, 2018. **231**: p. 115-120.
54. Sreenivasa Kumar, G., et al., *Ultra-range bimetallic Pt–Pd nanospheres deposited on reduced graphene sheet as efficient electrocatalyst towards electrooxidation of methanol.* Journal of Cluster Science, 2021. **32**: p. 27-36.

55. Wang, Y., et al., *Superior catalytic performance and CO tolerance of Ru@ Pt/C-TiO2 electrocatalyst toward methanol oxidation reaction.* Applied Surface Science, 2019. **473**: p. 943-950.

56. Xu, J., et al., *Hollow cobalt phosphide octahedral pre-catalysts with exceptionally high intrinsic catalytic activity for electro-oxidation of water and methanol.* Journal of Materials Chemistry A, 2018. **6**(42): p. 20646-20652.

57. He, C. and J. Tao, *Pt loaded two-dimensional TaC-nanosheet/graphene hybrid as an efficient and durable electrocatalyst for direct methanol fuel cells.* Journal of Power Sources, 2016. **324**: p. 317-324.

58. Bhavani, K.S., T. Anusha, and P.K. Brahman, *Fabrication and characterization of gold nanoparticles and fullerene-C60 nanocomposite film at glassy carbon electrode as potential electro-catalyst towards the methanol oxidation.* International Journal of Hydrogen Energy, 2019. **44**(47): p. 25863-25873.

59. Bredar, A.R., et al., *Electrochemical impedance spectroscopy of metal oxide electrodes for energy applications.* ACS Applied Energy Materials, 2020. **3**(1): p. 66-98.